A Fully Synthetic Type-I ELM Cycle Diagnostic Using Conventional O-mode Reflectometry

J. Vicente[1, a)], A. Cathey[2, b)], F. da Silva[1, c)], S. Heuraux[3, d)], M. Hoelzl[2, e)] and G. D. Conway[2, f)]

[1]*Instituto de Plasmas e Fusão Nuclear, Instituto Superior Técnico, Universidade de Lisboa, 1049-001 Lisboa, Portugal.*
[2]*Max-Planck-Institut für Plasmaphysik, Boltzmannstr. 2, 85748 Garching, Germany.*
[3]*Institut Jean Lamour, University of Lorraine-CNRS, F-54011 Nancy, France.*

[a)] Corresponding author: jvicente@ipfn.tecnico.ulisboa.pt
[b)] andres.cathey@ipp.mpg.de
[c)] tanatos@ipfn.tecnico.ulisboa.pt
[d)] stephane.heuraux@univ-lorraine.fr
[e)] mhoelzl@ipp.mpg.de
[f)] garrard.conway@ipp.mpg.de

Abstract. Significant advances in modeling and simulations for microwave reflectometry have been conducted in recent years. An example is the integration of improved numerical descriptions of magneto-hydrodynamics (MHD) instabilities, obtained from MHD codes, together with 2D full-wave codes to implement synthetic reflectometry diagnostics in realistic conditions. In particular, the nonlinear MHD code JOREK has been used previously together with the 2D full-wave code REFMUL, to assess the response of conventional O-mode reflectometry along a Type-I edge localized mode (ELM) crash. In this work, a similar framework and synthetic diagnostic set-up are considered but with an extended MHD simulation where a Type-I ELM cycle comprised of several ELM crashes is studied. This includes the self-consistent MHD evolution along inter-ELM periods, which was absent in the previous study. The reflectometer response at the mid-plane of the low magnetic field side is used to provide information about the behavior of density fluctuations along the full ELM cycle. The inter-ELM periods display density fluctuations in agreement with the ELM triggering mechanisms manifesting as reflectometry signatures which are identified with ELM precursors. The precursor signatures are observed a few milliseconds before a transition from linear to non-linear reflectometry regimes occurs, associated with the explosive onset of the ELM.

INTRODUCTION

The evolution of large-scale MHD instabilities in tokamaks can be modelled using non-linear MHD codes such as JOREK which solves the reduced visco-resistive single fluid MHD equations [1,2]. One important application of JOREK is to investigate the physics of ELMs in diverted tokamaks, as it allows simulation domains covering the main plasma, the scrape-off layer (SOL) and the divertor regions of X-point magnetic configurations (e.g. [3]). The large energy expelling Type-I ELMs require specific attention since their impact on the plasma facing components is such that they must be avoided in future reactors [4]. The first realistic simulations of multiple Type-I ELM cycles have been recently presented [5]. The self-consistent MHD evolution along inter-ELM periods was absent in previous studies that relied on arbitrary seed perturbations to model single ELM crashes [6]. The recent Type-I ELM cycle simulations reproduce realistic ELM sizes and timescales as well as retain the characteristic features leading to subsequent ELMs. The completeness of the ELM cycle modeling was an important step towards the complete understanding of ELM triggering mechanisms as well of the physics for ELM suppression and mitigation techniques.

On the other hand, the experimental characterization of MHD phenomena requires knowledge about the mean and fluctuating components of different plasma parameters. In a tokamak, a plasma mode can be generally characterized by a given toroidal mode number *n*, poloidal mode number *m* and frequency of rotation ω. Therefore, in a given poloidal cross-section of the torus, any plasma rotation may induce displacements on certain plasma density layers. The electron density fluctuations δn_e and n_e profiles can be measured using reflectometry techniques that are based on the propagation and interactions of electromagnetic waves in plasmas [7-10]. However, the plasma response to probing waves is complex and thus, to provide quantitative data interpretation, but also to assess and predict the performance of reflectometry diagnostics, reflectometry has found strong support in modeling activities (e.g. [11,12]). Synthetic reflectometry has been progressing and is currently based on solving Maxwell's equations using so called full-wave codes. REFMUL is a two-dimensional full-wave code, based on a finite-difference time-domain (FDTD) scheme, where the electric and magnetic fields are coupled to the electron density through the current density equation [13]. REFMUL allows to easily implement synthetic reflectometry diagnostics using ordinary mode (O-mode) waves. A simulation chain integrating the non-linear JOREK code and the full-wave REFMUL code was previously established and validated [14]. In this work, the full cycle of Type-I ELMs obtained from the JOREK simulations is considered. Here, a conventional reflectometer set-up at the mid-plane of the low magnetic field side (LFS) is employed in fixed frequency probing to provide information about the behavior of density fluctuations along the full ELM cycle. Particular attention is paid to the inter-ELM periods where novel ELM physics may be revealed with appropriate reflectometer settings, namely the chosen probing frequency f_o.

THE ELM CYCLE (IN A NUTSHELL)

The ELM cycle simulation obtained with JOREK was based on a stable and stationary post-ELM crash equilibrium reconstruction of a plasma discharge carried out at the ASDEX-Upgrade (AUG) tokamak [15]. It is important to note that the plasma had low triangularity shape and high density at the separatrix (approximately 40% of the Greenwald density), while other details of the experimental discharge and simulation can be found elsewhere ([5] and therein). The ELM cycle evolution can be seen in Fig. 1, where the magnetic energy of non-axisymmetric perturbations of all the non-zero toroidal mode numbers allowed in the simulation are displayed together with the incident power on the inner and outer divertor tiles.

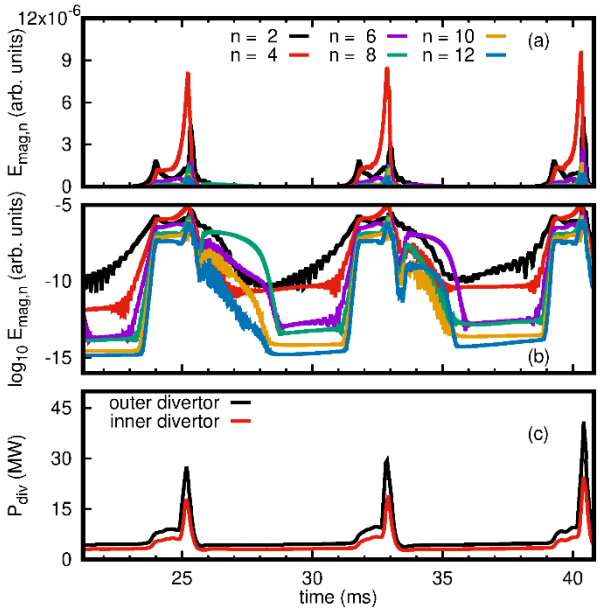

FIGURE 1. Magnetic energies of the non-axisymmetric perturbations of toroidal mode numbers $n \neq 0$ along ELM crashes and inter-ELM periods in linear (a) and logarithmic (b) scales. Power incident on the inner and outer divertor tiles (c).

Both the pressure gradient and the current density start-off by increasing at the plasma edge. A low frequency ELM precursor phase begins with an $n = 2$ perturbation becoming unstable. This can be seen in Fig. 1 a) and b)

starting at the earliest time displayed and then after each ELM crash (at t~21ms, t~28ms and t~36ms, respectively). This perturbation drives additional modes with larger toroidal mode numbers through non-linear interactions [16]. The growth rate of the precursors increases with time, driving the plasma through their instability threshold, eventually crossing a peeling-ballooning stability boundary. At this stage the precursors cause only a moderate increase in the power reaching the divertor, as can also be seen in Fig. 1 c). In this precursor phase, the low *n* modes act on the background axisymmetric plasma causing a gradual decrease of the pressure gradient and the current density. Due to an even faster slowing down of the plasma flow, ceasing to provide a stabilizing effect, an explosive growth phase of the magnetic energy of the perturbations follows. This is the onset of the ELM crash phase. After the end of the ELM crash, seed perturbations of non-negligible amplitude remain to become destabilized again with increasing pressure gradient and current density, repeating the ELM cycle, as described in more detail in [5].

THE SYNTHETIC REFLECTOMETER SET-UP

The electron density is the only plasma parameter required to model the plasma in the case of O-mode reflectometry, following the O-mode dispersion relation. Thus, the problem of integrating JOREK plasma descriptions with REFMUL simulations resumes to an adequate treatment of the electron density outputs from JOREK such that they can be included as two-dimensional density maps (describing a given poloidal cross section at a given time instant) in REFMUL. The general work flow regarding the code coupling requirements such as for coordinate transformation, data interpolation or boundary conditioning has been considered previously [14]. The methods employed to retrieve the in-phase $I(t)$ and quadrature $Q(t)$ reflectometry signals, as well as the amplitude $A(t)$ and phase $\phi(t)$, also follow a similar method to that described in previous work [17]. Also as before, the chosen region of interest (ROI) is comprised of a rectangular cross-section in the LFS, crossing the equatorial plane, bounded by the AUG cylindrical coordinate values Z = [-0.1, 0.1] m, and R = [2.12, 2.17] m. However, given the high density values at the separatrix and SOL, a smooth transition to vacuum was imposed by using an extended plasma density decay following a modified hyperbolic tangent profile in the radial direction. Examples of radial density profiles obtained at the central poloidal ROI position, from JOREK processed data are displayed in Fig. 2. The fully perturbed density data, directly obtained from JOREK at a given time instant (n_e, in black) and the estimated background plasma using a moving point-wise averaging over 80 consecutive density maps (in blue) are shown.

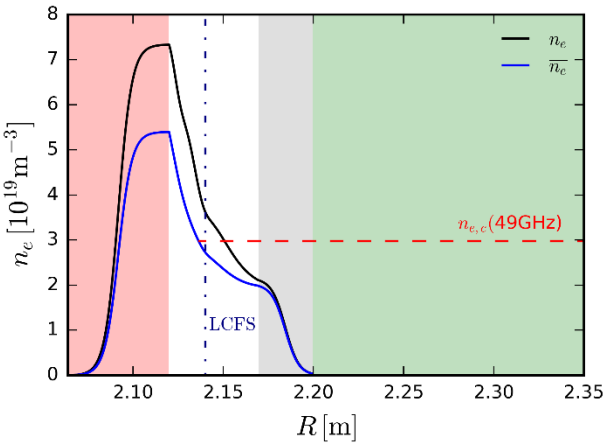

FIGURE 2. Radial electron density profiles from JOREK post-processed data used in REFMUL simulations. Profiles based on the fully perturbed data (black curve) and averaged data (blue curve) are shown. Color-shaded areas indicate different regions for: vacuum (green), modified hyperbolic tangent SOL transition (gray), JOREK data (white) and PML transition (red). The critical density layer for the probing frequency f_0 = 49 GHz is also displayed.

Different radial regions are indicated, including the transition to perfectly matched layers (PML) that are used for optimized boundary conditions at the edge of the simulation grid. The above JOREK data processing is independent of any particular reflectometer that is to be implemented. While a direct comparison with experimental data is not

envisaged in this work, we have chosen as a reference for this study a conventional O-mode reflectometer system installed at AUG [18]. This system is able to operate in fixed frequency currently covering the Q-band (33-49 GHz) and V-band (55-69 GHz) ranges. The simulations shown here were carried out with a probing frequency f_o = 49 GHz which is in the range of the experimental Q-band system. At this frequency, a cut-off condition is met at the critical (reflecting) density layer $n_{e,c} \approx 3\times10^{19}$ m^{-3}, which is indicated in Fig. 2. It should be mentioned that the cut-off position varies radially by a few centimetres along the ELM cycle, as the density perturbations evolve on top of the background plasma. Given that the wavenumber of ELM related structures (e.g. precursors) are much smaller than the probing wavenumber, the main contributions to the reflectometer signal should come from cut-off oscillations. In this case, the probing regions are in the vicinity of the Last Closed Flux Surface (LCFS). To further match the synthetic reflectometer with the experimental apparatus, a monostatic set-up with an H-plane horn antenna was considered, together with a vacuum distance of 22 cm from the antenna mouth to the plasma entry, and a half-power beam width ≤ 5.6 cm estimated from the radiation diagram in vacuum, at the average plasma cut-off distance.

SYNTHETIC FLUCTUATION REFLECTOMETRY SIGNALS

REFMUL simulations employing fixed probing frequency f_o = 49 GHz were run independently for each of the ≈1500 density maps obtained from JOREK, according to the methods previously mentioned and described in [14,17]. Each REFMUL run consisted of 120 thousand time-iteration points. Reflectometry time sequences were then built subsequently by sampling each REFMUL output data at the 90.000th iteration point, much larger than the corresponding time of flight and well into the stationary response regimes established at each REFMUL run. The time evolution of both $I(t)$ and $Q(t)$ signals recovered along the full ELM cycle is shown in Fig. 3 a).

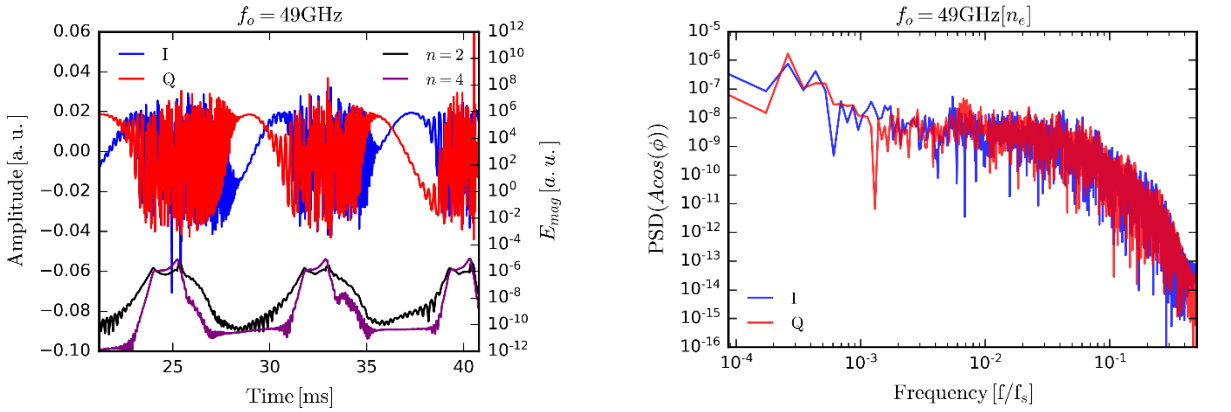

(a) (b)

FIGURE 3. Time evolution of synthetic $I(t)$ and $Q(t)$ reflectometry signals using fixed frequency probing at f_o = 49GHz along a ELM cycle obtained from JOREK simulations, where the magnetic energy of the n = 2 and n = 4 modes are also displayed (a). Spectra of the corresponding reflectometry signals whith the frequency axis normalized to the sampling frequency f_s (b).

Visual inspection of the reflectometry signals immediately reveals that the behaviour of the reflectometry response along inter-ELM periods and during ELM crash phases is quite different and noticeable. In particular, there is an onset of large amplitude variations preceding the peak of each ELM crash by a few milliseconds. Such amplitude variations are responsible for detrimental effects on the performance of reflectometry diagnostics during these plasma events, as observed previously with simulations [14]. In particular, with respect to occurrence of phase jumps and runaway effects on the phase $\phi(t)$ measurements, as can be seen in Fig. 4, where the reconstructed phase signals are displayed in the vicinity of a single ELM crash.

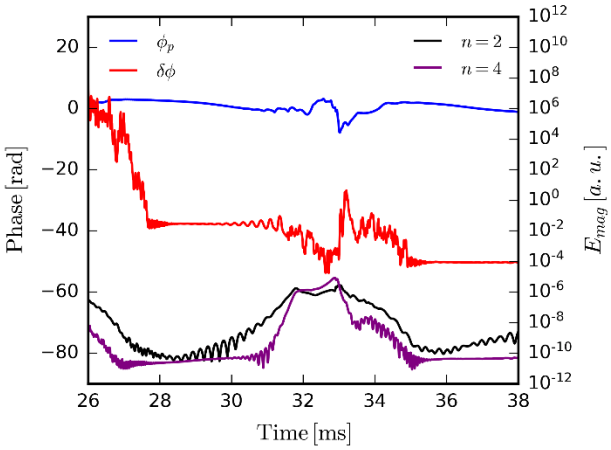

FIGURE 4. Time evolution of the phase of reflectometry signals in the vicinity of one ELM. The signals retrieved from independently probing the fluctuating (δ) and background ($_p$) plasmas, are displayed separately. The time evolution of the magnetic energy of the n = 2 and n = 4 modes is also displayed.

On the other hand, during the quiescent inter-ELM periods, which are now accessible in the new simulations, there is a harmonic oscillatory component of growing amplitude which appears leading to the more chaotic ELM onset oscillations. The oscillation growth appears to be a signature of the *n* = 2 ELM precursor activity described earlier since both the reflectometry oscillations and the magnetic energy of the *n* = 2 mode increase in correlated manner (see Fig. 4). Note that during the ELM crash phase, the large amplitude variations and associated phase effects remain only while the magnetic energy of the *n* = 2 mode is above a given threshold near the minimum that is observed in the inter-ELM periods.

On the other hand, the spectra of the reflectometry signals are broad and roll-over above a given frequency value, with approximately constant slope or spectral index, as displayed in Fig 3 b). However, there is also a signature of a more coherent feature in the vicinity of 7×10^{-3} [f/f_s] corresponding to a frequency of $f \approx 4$ kHz. This frequency value is in agreement with the wave period that can be estimated from the phase oscillations that we associate with the *n* = 2 ELM precursors. It is reasonable to assume that the transitions to non-linear responses, observed in the phase signals, occur when the ELM precursor amplitudes become large enough, which could be at moderate density fluctuation levels $\delta n_e/n_e$, similarly to what has been studied in the case of turbulence [19].

CONCLUSIONS

An extended JOREK simulation comprising several Type-I ELM crashes was used to study the conventional reflectometry response using a fully synthetic diagnostic. Probing from the LFS mid-plane with O-mode polarized waves in fixed frequency was considered for the reflectometer set-up, such that the plasma cut-off was positioned in the vicinity of the LCFS. During the ELM crash periods, reflectometry signals revealed several phase jumps and phase runaway effects. During inter-ELM periods, along the self-consistent MHD evolution, oscillatory reflectometry signatures were identified as ELM precursors. The precursor signatures, which have elsewhere been identified as ELM triggering mechanisms, were observed a few milliseconds before a transition from linear to non-linear reflectometry regimes occurs, associated with the explosive onset of the ELM.

In future studies, it should be possible to compare directly the mode frequency obtained directly from JOREK data with the frequency estimated by reflectometer signals. It is also desirable to extend the analysis and characterization of the precursor modes, for instance by extending the synthetic studies to other reflectometry techniques, such as those using Doppler or poloidal correlation set-ups.

ACKNOWLEDGMENTS

This work has been carried out within the framework of the EUROfusion Consortium, funded by the European Union via the Euratom Research and Training Programme (Grant Agreement No 101052200 — EUROfusion). Views and opinions expressed are however those of the author(s) only and do not necessarily reflect those of the European Union or the European Commission. Neither the European Union nor the European Commission can be held responsible for them. This work has also received financial support from the Luso-American Development Foundation and from FCT – Fundação para a Ciência e Tecnologia, I.P., in the frame of Estímulo ao Emprego Científico – Apoio Institucional – CEECINST/00102/2018/CP1567/CT0044.

REFERENCES

1. G.T.A. Huysmans and O. Czarny, Nucl. Fusion **47** 659 (2007).
2. M. Hoelzl, *et al*., Nucl. Fusion **61** 065001 (2021).
3. G.T.A. Huijsmans and A. Loarte, Nucl. Fusion **53** 123023 (2013).
4. T. Eich, *et al*., Nucl. Mater. Energy **12** 84-90 (2017).
5. A. Cathey, *et al*., Nucl. Fusion **60**, 124007 (2020).
6. A.F. Mink, *et al*., Nucl. Fusion **58** 026011 (2018).
7. M.E. Manso, Plasma Phys. Control. Fusion **B35** 141 (1993).
8. R. Nazikian and E. Mazzucato, Rev. Sci. Intrum. **66** 392 (1995).
9. C. Laviron, *et al*., Plasma Phys. Control. Fusion **38** 905 (1996).
10. E. Mazzucato, Rev. Sci. Intrum. **69** 2201 (1998).
11. F. da Silva, *et al*., Proc. 9th Int. Reflectometry Workshop – IRW9 (Lisboa, May 2009).
12. C. Lechte, *et al*., Plasma Phys. Control. Fusion **59** 075006 (2017).
13. F. da Silva, *et al*., Journal of Comp. Physics **203**, 467-492 (2005).
14. J. Vicente, *et al*., JINST **16** C12024 (2021).
15. H. Meyer, *et al*., Nucl. Fusion **59** 112014 (2019).
16. I. Krebs, *et al*., Phys. Plasmas **20** 082506 (2013).
17. J. Vicente, *et al*., Plasma Phys. Control. Fusion **62** 025031 (2020).
18. L. Cupido, *et al*., Rev. Sci. Instrum. **77** 10E915 (2006).
19. J. Vicente, *et al*., Rev. Sci. Instrum. **89** 10H110 (2018).